Hindawi
Advances in Civil Engineering
Volume 2024, Article ID 4268615, 21 pages
https://doi.org/10.1155/2024/4268615

Research Article

Experimental Investigation of Ductility in GFRP RC Beams by Confining the Compression Zone

Erfan Tahrirchi, Farshid J. Alaee, and Meysam Jalali

Department of Civil Engineering, Shahrood University of Technology, Shahrood, Iran

Correspondence should be addressed to Meysam Jalali; mjalali@shahroodut.ac.ir

Received 24 November 2022; Revised 3 March 2024; Accepted 30 April 2024; Published 18 May 2024

Academic Editor: Andreas Lampropoulos

Nowadays, building structures in corrosive environments requires some considerations. Being lightweight, high tensile strength, and corrosion resistance are the features that make fiber-reinforced plastic (FRP) bars an alternative component for longitudinal steel reinforcement of concrete. On the other hand, the linear elastic behavior of FRP bars, alongside the brittle behavior of concrete, makes brittle members without considerable ductility. In this paper, the effect of compression region confinement with CFRP sheets on the FRP-reinforced concrete beams was experimentally investigated. Eight GFRP reinforced beams with 2 m length, including one reference beam and seven confined beams, were constructed and tested under a four-point bending test. Based on the type of confinement, specimens are categorized into four groups. Flexural behavior improvements, including load carry capacity, energy dissipation capacity, and ductility, were observed in at least one specimen of each confined group. According to the results, the specimen that was spirally confined with a 30 mm ribbon width and angle of 10° had the best total energy absorption up to about 110% improvement in comparison to the unconfined specimen. On the other hand, vertically confined specimens with 50 mm ribbon width showed the highest improvement in ductility indices and load carrying capacity up to 60% and 11% in comparison to unconfined specimens, respectively. Due to concrete compression zone fractures in flexural failure mode, the over-reinforce method is considered the design philosophy. Results indicate that regardless of the confinement type (discrete vertical, discrete spiral, or continuous spiral confinement), there is an optimal amount for width, blank space between ribbons, and depth of confinement to achieve the best flexural behavior.

1. Introduction

A substantial number of reinforced concrete (RC) buildings are constructed in aggressive and humid environments around the world. Due to the existence of chloride ions in such environments, most buildings are vulnerable to corrosion by aging. Different methods have been suggested by researchers to overcome this problem. An efficient method to eliminate the corrosion was replacing steel bars with fiber-reinforced plastic (FRP) bars. In this regard, FRP is a suitable material due to its nonmagnetization features, high-strength capacity-to-weight ratio, lightweight, prominent durability, low conductivity to electrical and electromagnetic, and long-term resistance against corrosion [1–6].

Composite materials known as FRP contain glass, carbon, aramid, or basalt fibers embedded in a matrix (resin). FRPs could be used as bars to reinforce a concrete section, as tendons for posttensioning [7], and as sheets for rehabilitation, retrofitting, and strengthening of structural members [8]. FRP in the form of sheets suffers from some premature failures, such as debonding and delamination. Many researchers conducted various studies to overcome these failures [9–11]. They considered different mechanical properties of FRP, such as strength, modulus of elasticity, and thickness of FRP, to study how these parameters affect the failure mode. Retrofitting with FRP provides anisotropic features, such as high tensile strength but weakness in compression and shear. FRP bars have mostly lower modulus of elasticity than steel. However, the linear stress–strain behavior, up to the failure, makes sudden fracture without any plastic zone. So, poor ductility with low deflection and brittle failure is caused by FRP usage in the RC beams [12–15]. Hence, an over-reinforcement philosophy design is suggested in FRP-RC beams to produce some amount of ductility. This

Table 1: Concrete mix design.

Mix proportion	Cement	Coarse aggregate	Fine aggregate	Water	Expansive pro-grout 105
Weight per cubic meter (kg/m^3)	373.77	717.2	961	228	1.8

Table 2: Compression test result of cubic concrete specimens.

Cubic concrete specimens	S1	S2	S3
Compressive strength (MPa)	24.45	24.20	23.79

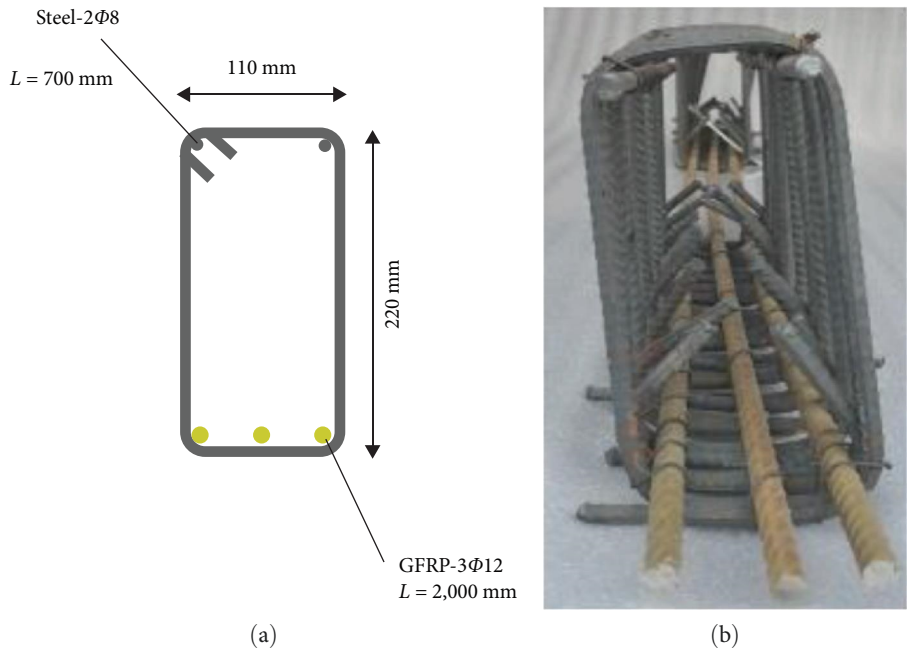

Figure 1: Stirrups of specimens: (a) schematic of stirrups; (b) used stirrups.

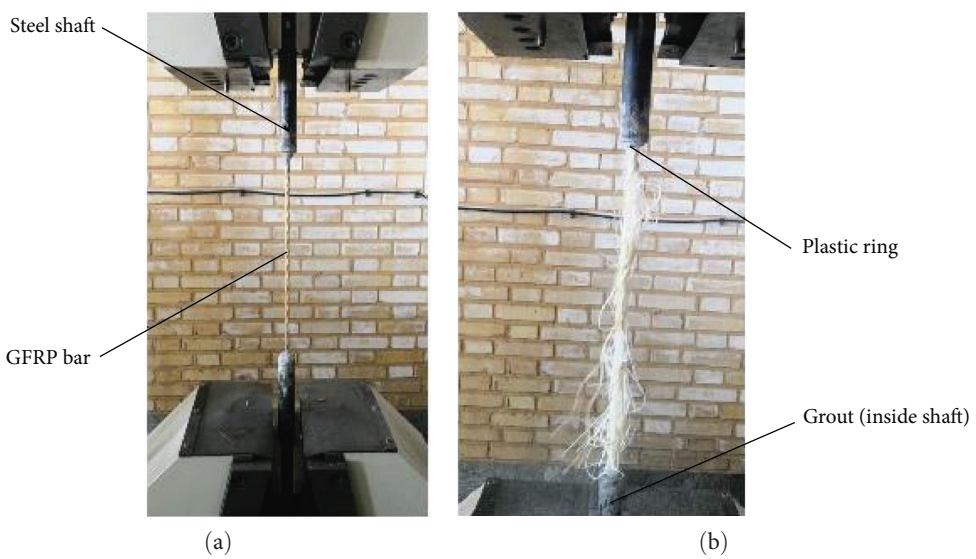

Figure 2: GFRP bar tensile strength: (a) before tensile test; (b) after tensile test.

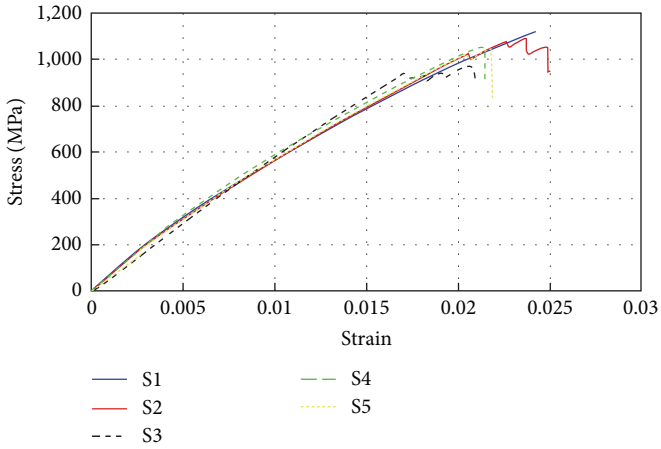

Figure 3: Stress–strain curves of five tensile GFRP specimens.

Table 3: Properties of GFRP bars.

Specimens	$\text{Stress}_{\text{max}}$ (MPa)	Strain_{u}	E_{u} (MPa)
S1	1,120.71	0.0243	46,164.35
S2	1,093.61	0.0237	46,057.77
S3	973.82	0.0208	46,854.00
S4	1,057.41	0.0214	49,414.42
S5	1,048.03	0.0218	48,073.21
Ave.	**1,058.72**	**0.0224**	**47,312.75**

philosophy provides more load-carrying capacity compared with steel-RC beams [16, 17].

Several approaches have been studied as effective solutions to provide more ductility in FRP-RC beams. The first approach has suggested the usage of FRP with different types of fiber or in combination with steel bars. Studies revealed that the ductility index of hybrid FRP-RC beams was close to that of the beams reinforced by steel. The combination of steel and FRP bars for reinforcement presented good improvements in flexural behavior regarding deflection, ductility, curvature, and crack width. Such a manner could provide an acceptable design for an RC beam; however, the corrosion issue was still standing [18–21]. The second approach for improving the ductility of FRP-RC beams was the addition of fibers to concrete and making fiber-reinforced concrete (FRC). Test results showed that FRP/FRC beams had better compression properties, larger compressive strain, ductility, deflection, and flexural strength than FRP-RC beams. Polypropylene, steel, and glass fibers were used in the concrete mixture and tested. Researchers found out that steel fibers have better performance and can improve the flexural strength and ductility by up to 50% and 17%, respectively [22–24]. It should be noted that in the case of using steel fibers, the corrosion issue remains unsolved!

In another study, the whole or part of the beam concrete was replaced by engineered cementitious composite (ECC) to improve the flexural behavior. ECC is a kind of ultra-ductile composite with the ultimate tensile and compressive strain of about 200–700 times and twice greater than that of

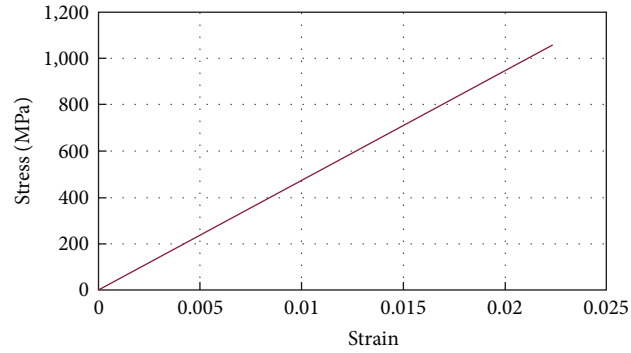

Figure 4: Design stress–strain behavior curve of GFRP bars.

conventional concrete, respectively [25]. FRP-reinforced ECC beams behaved more desirable than FRP-RC beams in terms of deformability, load-carrying capacity, ductility, and crack control in flexure. In addition, the usage of the ECC matrix made FRP bars more efficiently utilized in comparison with ordinary concrete [26–29]. Of course, ECC is much more expensive than the conventional concrete.

Employing compression-yielding (CY) blocks in the compression zone of the beams was another method to improve the flexural behavior of over-RC beams. CY block could be in any ductile shape and material like steel. Studies showed that CY can produce great ductility in the beams if the optimum size, shape and strength of the CY block is found [30–34]. In the case of using steel CY blocks, again the issue of corrosion is raised!

In another line of research, the effects of confined structural concrete members using FRP sheets were investigated. It was found that confining is an efficient method to improve the compressive behavior of concrete. The application of confinement not only increases the compressive strength of concrete, but it can also dramatically improve the ultimate compressive strain of concrete [35–40]. Campione [41] has experimentally and analytically investigated square cross-section concrete prisms wrapped with CFRP sheets. A total of 22 specimens with square cross-sections of 150 mm side with lengths of 150, 300, and 450 mm were cast and tested under a compression test machine. The investigated parameters were the wrapping configurations with discontinuous vertical and horizontal strips, effects of specimen corner reinforcement by single strips, layer number, and specimen length. Test results clarified that the bearing capacity of CFRP-wrapped specimens with one and two layers increases up to 27% and 42%, respectively. Wu et al. [42] studied the flexural behavior of under-RC beam that CFRP sheets bonded at the tensile surface of the beam while GFRP sheets were hoop-directionally wrapped to bear the shear load and provided confinement to the whole concrete core and also to prevent debonding of CFRP sheets. They cast six beam specimens with 200, 150, and 2,000 mm of sides and tested them under four-point bending. They found that in the lack of axial load (pure flexural load), the effect of FRP confinement is negligible.

This study presents an innovative idea of improving the flexural behavior of FRP-RC beams by confining the

Table 4: Properties of CFRP sheets [49].

Product name	Description	Thickness (mm)	Tensile strength (MPa)	Elasticity modulus (GPa)	Elongation at break	Areal weight (g/m^2)
QUANTOM® Wrap 300 C	High-strength carbon UD fabric	0.168	4,950	235	1.9%	304

Table 5: Properties of CFRP sheet adhesive (EPR3301) [49].

Description	Value
Color	Concrete gray (mixed)
Density (at 25°C)	1.5 kg/l (mixed)
Bonding strength	>3.5 MPa (concrete failed)
Compressive strength	95 MPa (7 days) at 35°C
Tensile and flexural strength	>30 MPa
Service temperature	−35 to +65°C
Full cured	After 7 days (at 25°C)
Working time/pot life	60 min (25°C)

concrete in the compression zone using FRP sheets. There is no steel in the proposed concept, and the corrosion concern has been eliminated. The authors aim to improve the ductility of FRP-RC beams by taking advantage of confined concrete, which is strong and ductile. The only limitation of this study was the unbendable characteristic features of FRP bars, so that the stirrups could not be made of FRP and steel bars were used instead. In different methods, stirrups could be eliminated [43]. Of course, since all the beams failed in flexure, this cannot make any difference in the results and discussions.

2. Materials and Methods

In this study, the experimental tests were carried out in two phases: tests on the materials and beam specimens. To attain consistency of test condition, a single concrete mix, the same GFRP bars, and identical CFRP sheets were used for all beams.

2.1. Concrete. The concrete mixture design of this research was considered as ACI 211.1-91 [44] suggested for 25 MPa strength on the 28th day. The concrete material constituents include ordinary Portland cement type II, aggregates (maximum size 9.5 mm designed based on ASTM C33-2013 [45], water, and expansive admixture (Pro-Grout 105 produced by Shahrood Mohafez Chemical Industries). These materials were mixed by proportions presented in Table 1.

To study the compression behavior of concrete, based on BS EN 12390 [46], three cubic specimens with 150 mm side each were molded alongside beam specimens. To cast concrete, dry materials were mixed first. Then, water was gradually added and mixing was continued until a uniform mix was made. Concrete was placed in the molds and cured for 28 days at ambient temperature before testing. The compressive strength of concrete was obtained by a load-control compression test on cubic concrete specimens (see Table 2). The average compressive strength of concrete and the standard deviation were 24.15 MPa and 0.27, respectively.

2.2. Reinforcement Bars. In this study, two types of bars have been used. Steel reinforcement bars (known as AIII) have been used to establish stirrups since GFRP bars cannot be bent in place. On the other hand, this research studies the flexural behavior of beams. Thus, stirrups resist shear failure mode and have negligible effects on the flexure. As shown in Figure 1, ribbed rebars 8 mm in diameter with 135° of hook, 110 mm width, and 220 mm height were constructed.

To determine the mechanical properties of the longitudinal GFRP bars supplied by Abar Saze Aryana Company, their tensile strength was measured. This test was performed according to ASTM D7205/7205M-06 [47] and ISO 10406-1-2008 [48], as shown in Figure 2. The tensile strength was obtained based on five specimens with a diameter of 7.5 mm and a length of 900 mm. The GFRP bar specimen includes one steel shaft as a grip on both sides, which sticks to GFRP by grout. Test results of specimens are presented in Figure 3 and Table 3; meanwhile, the average stress–strain curve of the GFRP bar is illustrated in Figure 4. The average tensile strength, ultimate strain, and elastic modulus were found to be 1,058 MPa, 2.2%, and 47.3 GPa, respectively.

2.3. CFRP Sheets. To provide confinement in the compression zone of beams, CFRP sheets and their adhesive (EPR3301) were supplied from QUANTOM company [49]. The adapted properties of CFRP sheets and their adhesive from the catalog are presented in Tables 4 and 5, respectively.

3. Main Specimens Preparation

To assess the effectiveness of compression zone confinement for improving the ductility of FRP-RC beams, a set of eight FRP-RC beam specimens was designed. All specimens had identical dimensions and internal reinforcement arrangement, as shown in Figure 5. All eight beams selected for testing were considered at half scale as 2,000 mm × 250 mm × 140 mm (length × height × thickness) with 1,800 mm span to avoid supports crushing. Length consideration assured flexural failure occurrence instead of shear failure. Reinforcement distribution in all beam specimens includes three longitudinal GFRP bars with 12 mm of diameter located at 220 mm depth from the top, 17 steel stirrups with 8 mm diameters and 40 mm space, fixed by two steel bars with 8 mm diameter in the top, located in one-third of span in each side. The inflexibility features of GFRP bars caused the utilization of steel stirrups instead of GFRPs. The height of the confined zone was selected at 75 mm (in specimens with rectangular confinement cross-section) in such a way that its ratio with beam thickness was below 2, as

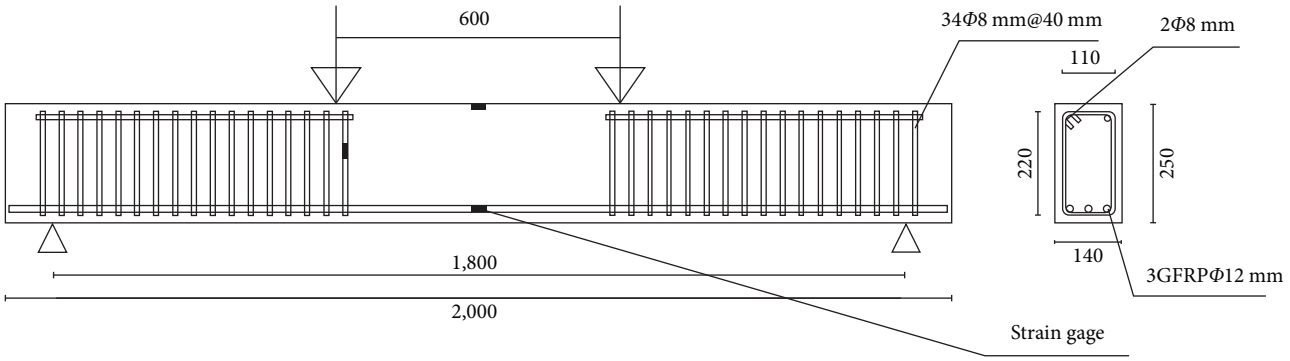

Figure 5: Reinforcement details of beam specimens (all dimensions in mm).

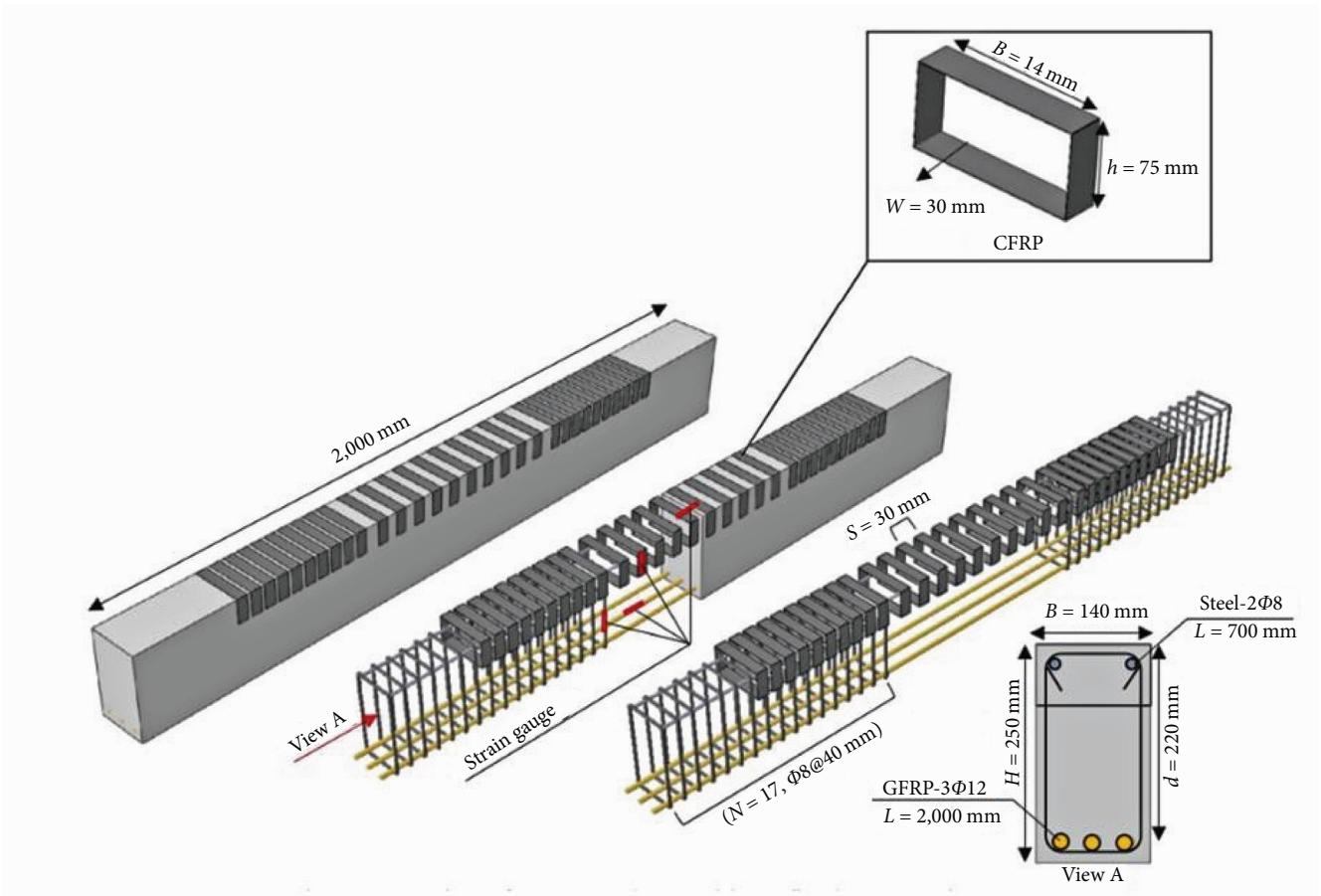

Figure 6: 3D model of DVR-W30 in confinement and reinforcement distribution.

Table 6: Properties of beams.

Groups	Specimens	Confinement type	Width 1[a] (mm)	Width 2[b] (mm)	Space 1[c] (mm)	Space 2[d] (mm)	Angle[e] (degree)
Group1	RB	—	—	—	—	—	—
Group2	DVR-W30	Discrete vertical	30	20	30	20	0
	DVR-W50		50	20	50	20	0
Group3	DSR-A10-W30	Discrete spiral	30	20	45	55	10
	DSR-A20-W30		30	20	126	136	20
	DSR-A30-W30		30	20	218	228	30
Group4	CSR-SR-W20	Continuous spiral	20	20	100	100	16
	CSR-SC-W20		20	20	100	100	16

[a]Width of CFRP ribbons at one-third of midspan; [b]Width of CFRP ribbons at one-third of side span; [c]Space between CFRP ribbons at one-third of midspan; [d]Space between CFRP ribbons at one-third of side span; [e]Angle of CFRP ribbons.

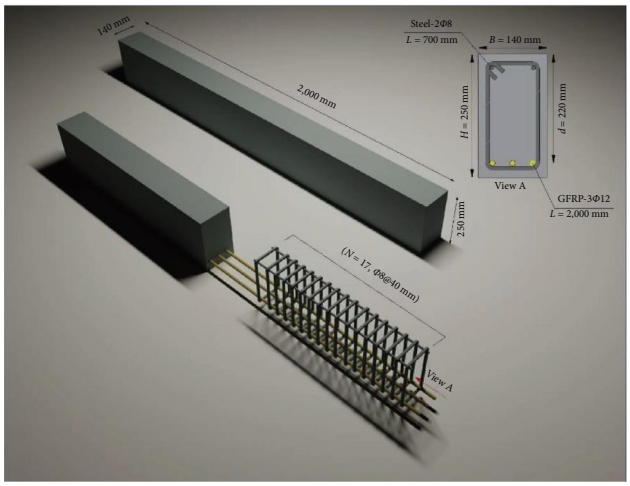

(a)

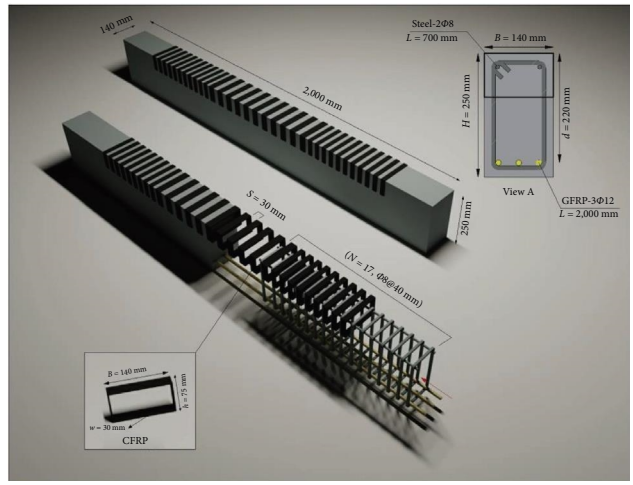

(b)

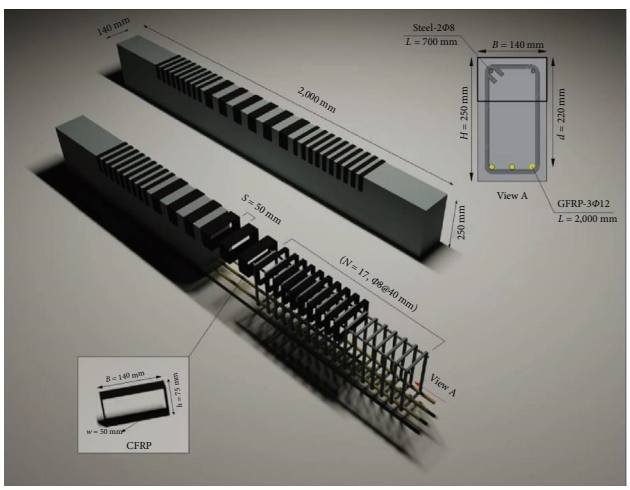

(c)

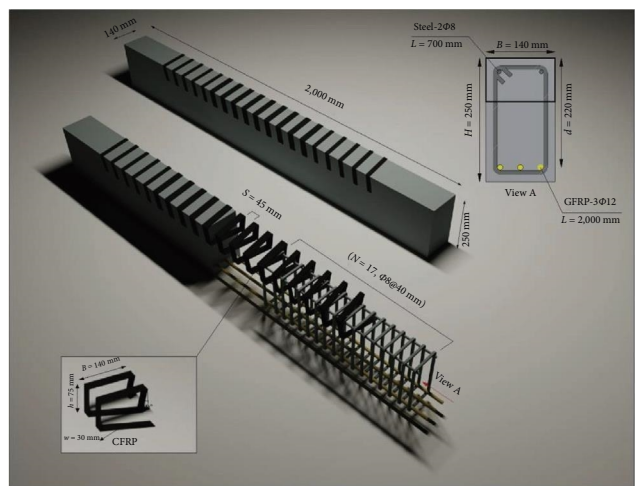

(d)

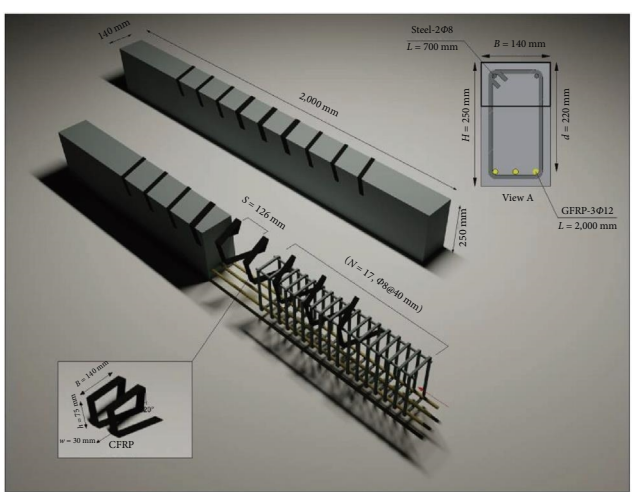

(e)

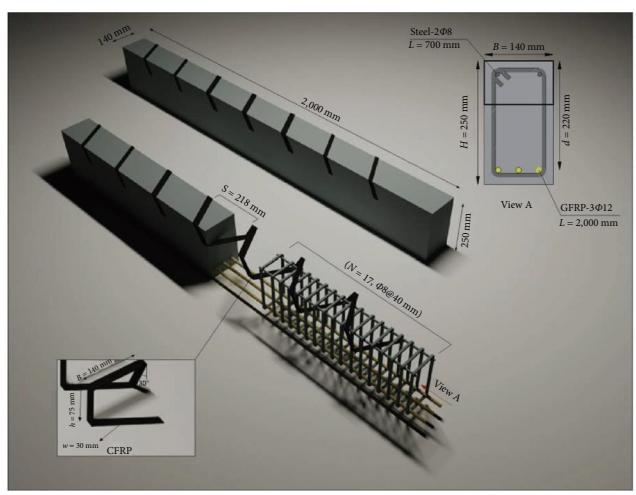

(f)

Figure 7: Continued.

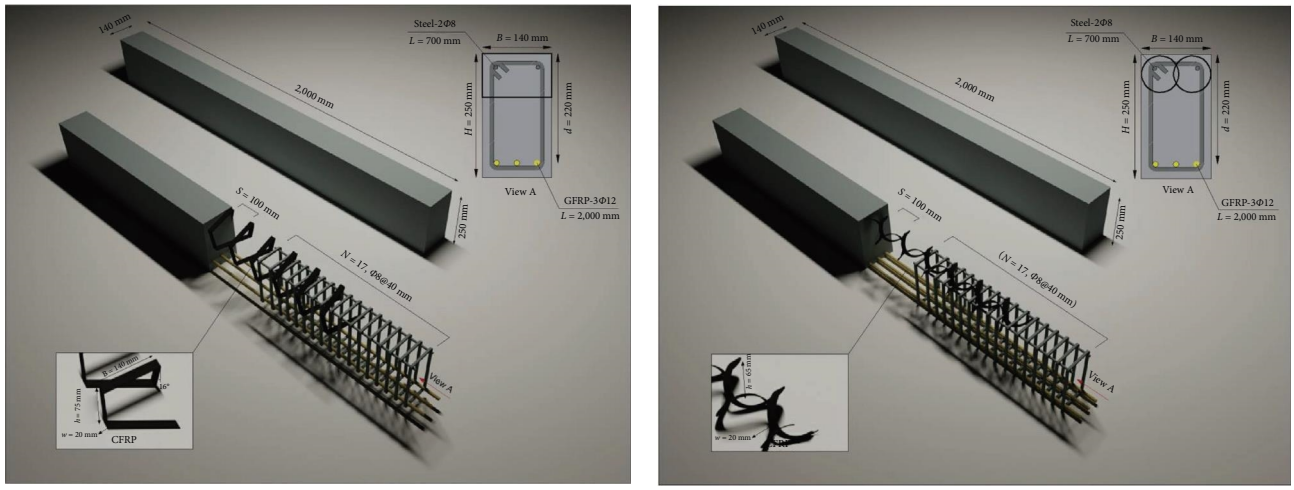

(g) (h)

FIGURE 7: 3D model of specimens in confinement and reinforcement: (a) RB; (b) DVR-W30; (c) DVR-W50; (d) DSR-A10-W30; (e) DSR-A20-W30; (f) DSR-A30-W30; (g) CSR-SR-W20; (h) CSR-SC-W20.

ACI 440.2R.17 [50] required. On the other hand, the height of the confined zone should consider where the neutral axis is located. Hence, the confined area stays in compression, during the test process. In addition, four strain gauges, attached to the middle of the central longitudinal GFRP bar, mid-height of the stirrup, the top surface of concrete, and the side surface of CFRP sheets, were embedded in concrete (see Figure 5). These gauges, produced in Tokyo Sokki Kenkyujo Co., were used to gather strain data of different components during the test process. The 3D model of reinforcement and confinement distribution of DVR-W30 (with Discrete Vertical CFRP Ribbons in 30 mm width) is illustrated in Figure 6.

Eight specimens categorized into four groups were cast and tested. Each beam is defined by letters and numbers indicating the continuity of CFRP ribbons and their direction, the angle of ribbons relative to the vertical axis (if needed), or the cross-section shape and width of confinement ribbons. The first group contained one concrete beam without confinement as reference beam (RB). The second group included two beams confined with discrete vertical CFRP ribbons in 30 mm width (DVR-W30) and 50 mm width (DVR-W50), respectively. The third group contained three beams with discrete spiral CFRP ribbons confinement with 30 mm width and angle of 10° (DSR-A10-W30), 20° (DSR-A20-W30), and 30° (DSR-A30-W30), respectively. The final group included two beams confined with continuous spiral CFRP ribbon in 20 mm width and circle cross-section (CSR-SC-W20) and rectangle cross-section (CSR-SR-W20). In all confined specimens, to prevent any interference between the stirrups and the confinement ribbons in one-third of the side spans, the width of the confinement ribbons was considered to be 20 mm with the same center-to-center distance between the ribbons or less depending on the stirrup locations. A summary of the specimen confinement characteristics is presented in Table 6 and Figure 7. Reinforcements and molds were provided in the same manner for all beams. Then, confinement ribbons are set at exact places between reinforcements. To protect the ribbons from being smeared by concrete where ribbons are located outside of concrete, polyfoams were placed between the concrete and the exited ribbons and stuck to the mold. To keep the uniformity of the test conditions, polyfoams were used in all specimen molds. Finally, concrete with 25 MPa target strength and mix design presented in Table 1 was cast in place and cured for 28 days before testing. After demolding the specimens, the exited ribbons were precisely glued to the specimen surfaces by an epoxy resin. The final thickness of FRP sheets with adhesive reached 1 mm.

The manufacturing of confined FRP-RC beams in this study was based on embedded CFRP sheets. At first, steel stirrups and longitudinal GFRP bars were bent and fixed at their designed places (Figure 8(a)), then strain gauges sticked at the middle of the GFRP bar and one of the stirrups. The required width and length of CFRP ribbons based on the designed beam were calculated and cut from the roll. Then, ribbons are attached in place due to its design location (Figure 8(b)). Since CFRP ribbons of CSR-SC-W20 and CSR-SR-W20 had to be formed and totally embedded in concrete, CFRP ribbons wrapped all around specific precast molds (Figure 8(c)). To stabilize the CFRP-wrapped form of CSR-SC-W20 and CSR-SR-W20, two-component epoxy resin was mixed, and the surface of CFRP ribbons was glued (Figure 8(d)). After the resin was completely set, shaped CFRP ribbons were braided into the reinforcement (Figure 8(e)). To fit the CFRP ribbons and prevent getting soaked while the concrete been cast, some polyfoams were placed to become a barrier between the CFRP ribbon's sides and concrete. To keep the equality condition of tests, polyfoams were placed in all specimens, even on those that were not necessary, like RB (Figure 8(f)). Then, molds were assembled and balanced. To prevent adhesion between mold and concrete beams, molds were smeared with mold oil. Thus, easy concrete removal was provided (Figure 8(g)). All reinforcements were placed in molds and controlled correction of reinforcement and CFRP ribbons (Figure 8(h)). Finally, based on Table 1, concrete was mixed meticulously and cast in molds. To compact the concrete and remove air that gets stuck in it, a vibration device was provided (Figure 8(i)). The

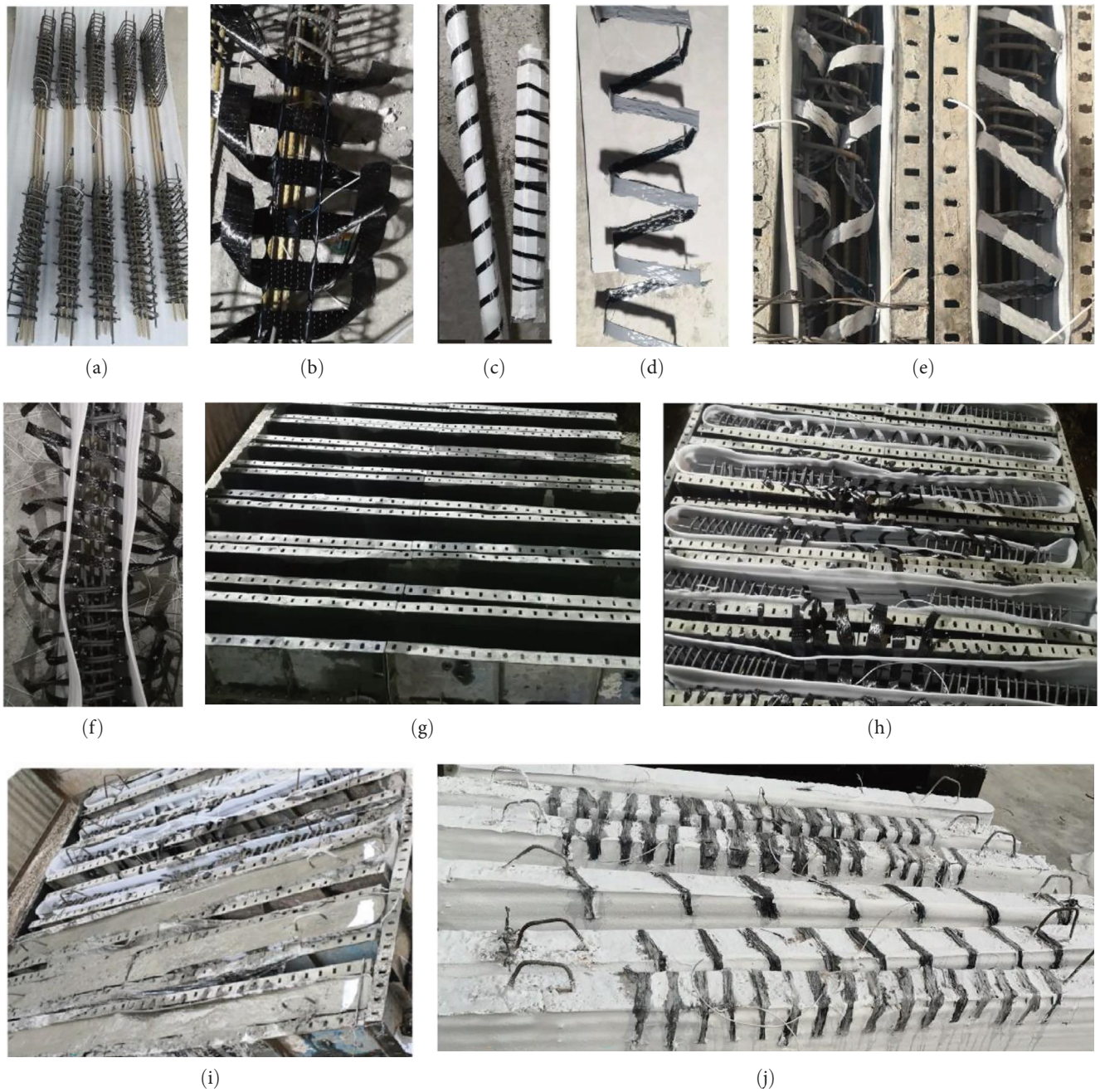

Figure 8: Manufacturing process of specimens: (a) reinforcing; (b) ribbons set in place; (c) molded confinement of group 4; (d) the confinement of CSR-SR-W20; (e) confinement of Group 4 braids into the reinforcement; (f) polyfoams placed; (g) molds; (h) reinforcement placed into the molds; (i) casting concrete; (j) specimens after curing.

curing process took long for 28 days, and specimens had to stay wet in the whole curing period. After 7 days, specimens were unmolded, and CFRP ribbons were glued to three sides of specimens as designed. On the 28th day, all specimens were painted in white color to better crack observation during the test process (Figure 8(j)).

4. Test Setup

As shown in Figure 9, the four-point bending test machine was supported by the foundation in the laboratory's strong floor. The test loading instruments consisted of a 1,000 kN hydraulic jack with a load cell. Two point-loads with 600 mm distance were applied to the specimens through a spreader beam. The load was exerted on the beams in displacement-control mode at the rate of 1.7 mm/min. To avoid overcoming of bearing high stress in supports, 100 mm spacing was considered from each end of the beams. Thus, the clear span of the specimens was 1,800 mm. The mid-span deflection was measured by an LVDT instrument. The records of the load cell, LVDT, and strain gauges were collected by a data logger throughout the tests.

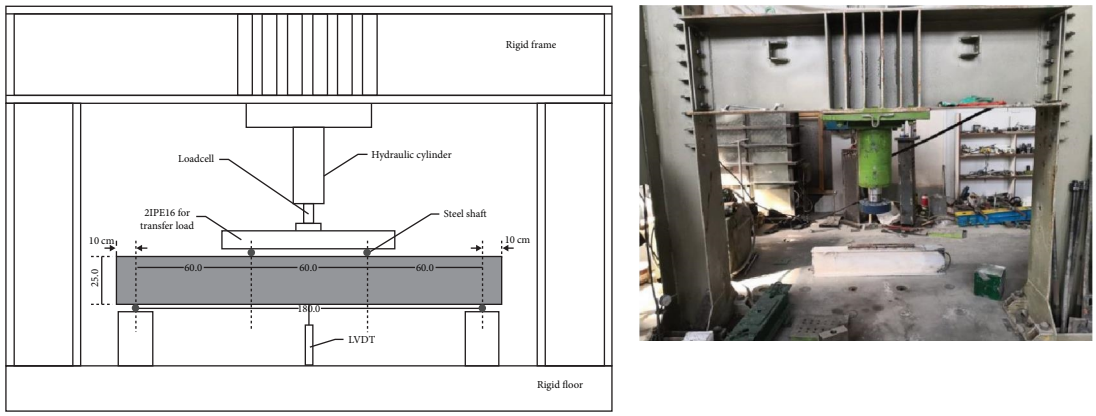

(a) (b)

Figure 9: Test setup and instruments: (a) schematic of test setup and instruments; (b) test setup and instrument.

5. Results and Discussions

In this section, the experimental test results of confined and unconfined specimens are presented. In addition, the load-deflection curves, crack patterns, energy dissipations, ductility indices, load capacity, and strain gauge results are compared.

5.1. Observations and Cracking Pattern. According to experimental observations of the RB (Group1), the beam had linear behavior till the first crack appeared at about 14.7 kN load. By increasing the load, the first cracks appeared vertically at one-third of the middle span in flexural mode. At 39.2 kN load, oblique cracks had been developed to one-third of the side span in flexural mode. As more load increased, more cracks developed, until the load reached the maximum amount of 113.78 kN. So, a crack occurrence at the top of the cross-section at the middle span caused the failure of the beam.

In the DVR-W30 of the second group, which was confined with discrete vertical ribbons of CFRP sheet, first cracks showed up after about 19.6–49 kN load at one-third of the middle span vertically in flexural mode, then the oblique cracks created in one-third of side span. Development of cracks was continued at the whole span till loadcell showed 123.13 kN load. At this moment, horizontal cracks were propagated where CFRP sheets exited from inside of concrete at one-third of the middle span. The cracks revealed issues at continuity between confined and unconfined zones. Thus, this beam failed before confinement came into action. The DVR-W50 of the second group had linear behavior with no sign of cracks up to 19.6 kN load. After that, the first vertical cracks showed up at one-third of the middle span in flexural mode up to 34.3 kN, and then the cracks developed to one-third of the side span. A high rate of crack development in this specimen was observed, as the whole span had cracks when the load cell showed 58.8 kN load. Afterward, the development of the cracks continued until the specimen failed at 126 kN load. In the failure process, cracks in compression concrete started at the median space between two CFRP ribbons, while the confined zone showed good resistance against cracks. Thus, cracks grow lower than CFRP confinement and fractures occur in areas with higher depth than the confined zone.

In the third group with discrete spiral ribbon confinement, DSR-A10-W30, the first crack showed up at about 14.7 kN load at the middle one-third of the span; after the load reached 24.5 kN, cracks were observed at one-third of the span side, but these cracks did not reach the supports. In the following, after 73.5 kN load, cracks grow to the confined area, then horizontal cracks were observed in the confined zone and below. Finally, the beam failed at the middle height of the beam below the confined zone before the confined area failed. In specimen DSR-A20-W30, first cracks occurred at about 11.76 kN load in the middle one-third span, then by reaching the 34.3 kN, cracks propagated to the sides of the span and arrived near supports in about 107.8 kN load. Eventually, horizontal cracks showed up where CFRP ribbons exited from the concrete. After a while, horizontal and vertical cracks joined together and caused the beam fracture. The first cracks in specimen DSR-A30-W30 of the third group occurred in about 14.7 kN at the one-third of the middle span. After 39.2 kN, cracks diagonally developed to one-third of the side span until the beam failed at 108.12 kN load. In this specimen, failure of the beam was observed at the top of the middle span, seeming like confinement did not come into action.

In the fourth group with continuous spiral CFRP ribbons, CSR-SR-W20 first cracks occurred at about 14.7 kN load in one-third of the middle span. At about 29.4 kN, diagonal cracks showed up in one-third of the sides span and continued up to 98 kN load. Then, the crack width increased by reaching 116.81 kN load in one-third of the middle span. After a while, horizontal cracks were observed in the confined zone and grew below the confined zone. So, when horizontal and vertical cracks joined together, the beam failed at the area below of the confined zone. In the final specimen, known as CSR-SC-W20, the first cracks were seen at 19.6 kN load at one-third of the middle span. By reaching 29.4 kN load, cracks developed to one-third of the sides span. By reaching 113.94 kN, vertical cracks grew at the beam height but did not enter the confined zone. Then,

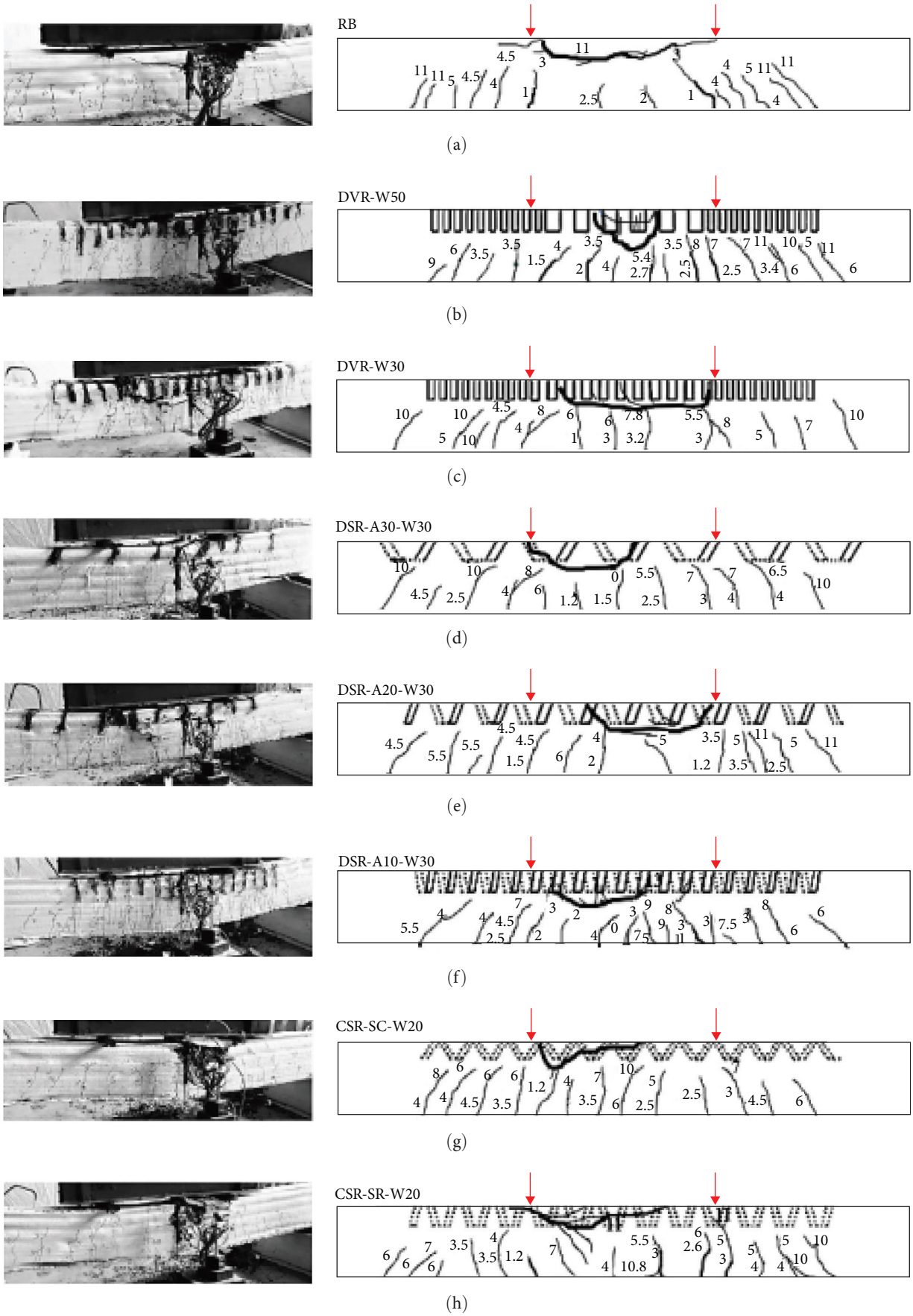

Figure 10: Cracking pattern of specimens. (a) RB specimen, (b) DVR-W50 Specimen, (c) DVR-W30 Specimen, (d) DSR-A30-W30 Specimen, (e) DSR-A20-W30 Specimen, (f) DSR-A10-W30 Specimen, (g) CSR-SC-W20 Specimen, and (h) CSR-SR-W20 Specimen.

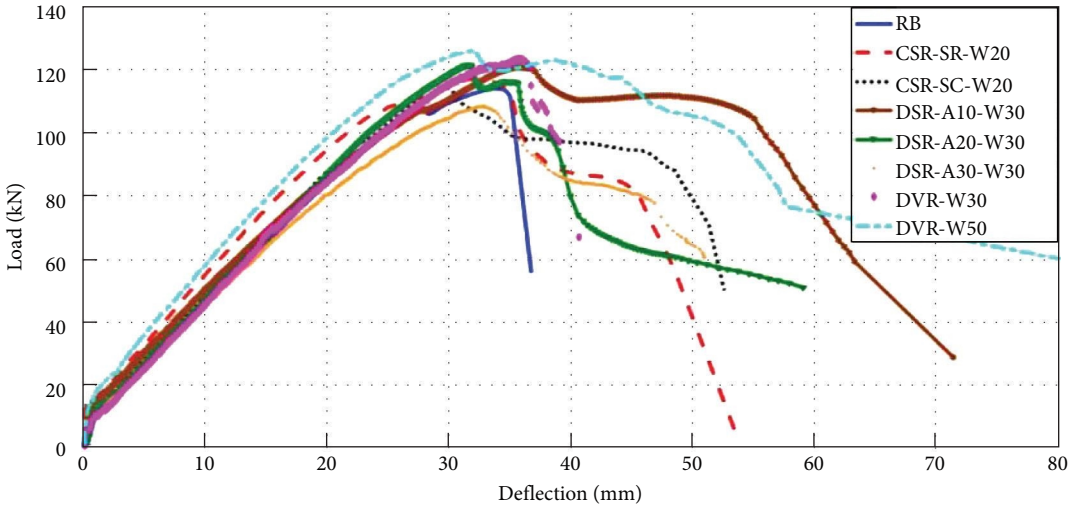

Figure 11: Load-deflection curves of all eight specimens.

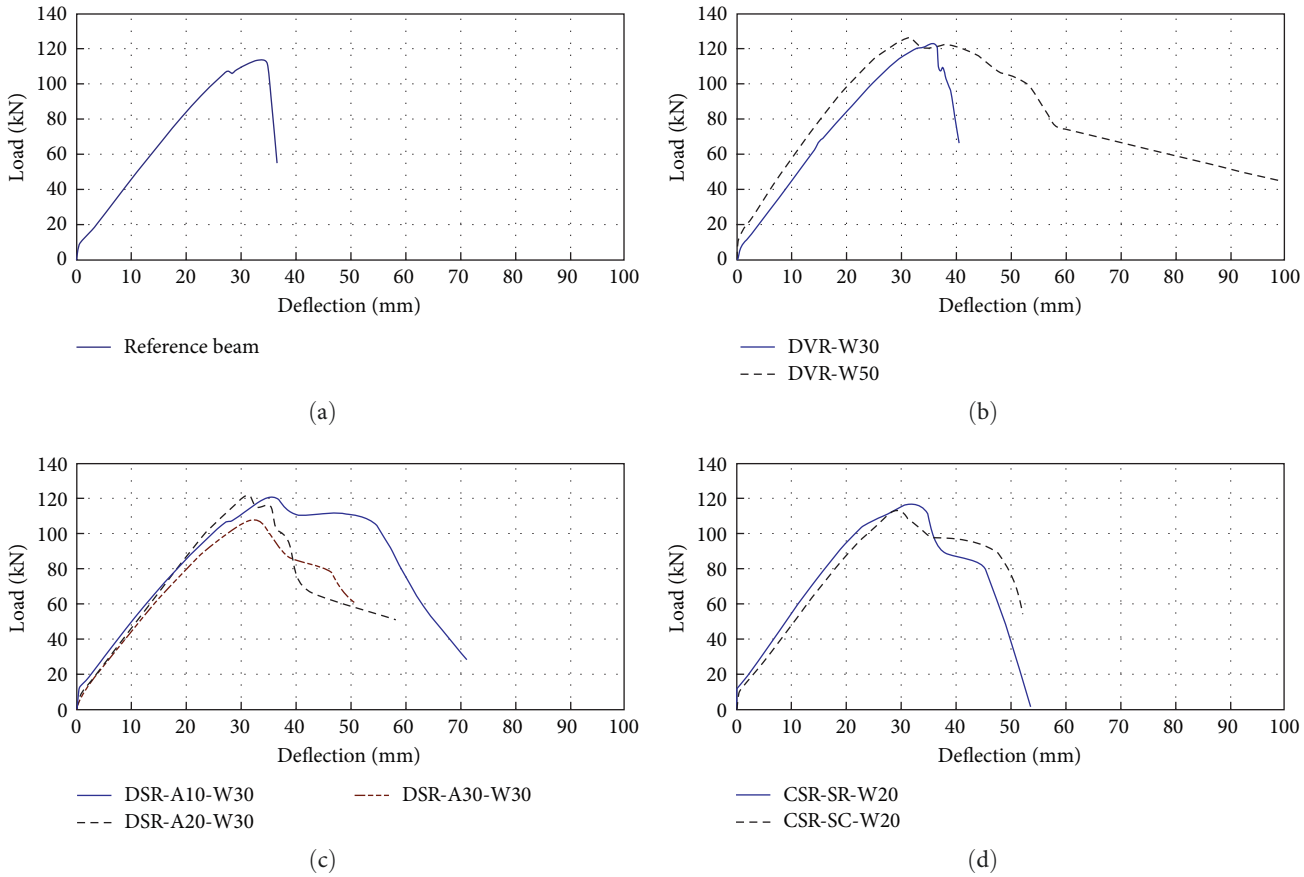

Figure 12: Load-deflection curves of each group: (a) load–deflection curve of Group 1; (b) load–deflection curve of Group 2; (c) load–deflection curve of Group 3; (d) load–deflection curve of Group 4.

horizontal cracks occurred at the top of the beam height. Finally, when the horizontal and vertical cracks joined together, the fracture occurred between two adjacent ribbons and below the confined area.

Generally, the compressive zone fracture in flexural failure mode was observed in all eight specimens. The cracking pattern of all specimens is presented in Figure 10. According to this figure, a great number of cracks are observed in the

Table 7: Load capacity and stiffness of specimens.

Group	Specimen	Load capacity (kN)	Stiffness
Group 1	RB	113.78	4.17
Group 2	DVR-W30	123.13 (+%8.21)[a]	4.13 (−%1.04)
	DVR-W50	126.02 (+%10.75)	4.99 (+%25.25)
Group 3	DSR-A10-W30	120.53 (+%5.92)	4.19 (+%0.45)
	DSR-A20-W30	121.191 (+%6.5)	4.31 (+%3.34)
	DSR-A30-W30	108.12 (−%4.97)	3.97 (−%4.72)
Group 4	CSR-SR-W20	116.81 (+%2.66)	4.85 (+%16.34)
	CSR-SC-W20	113.94 (+%0.13)	4.41 (+%5.71)

[a]Percentages of changes compared to the reference beam.

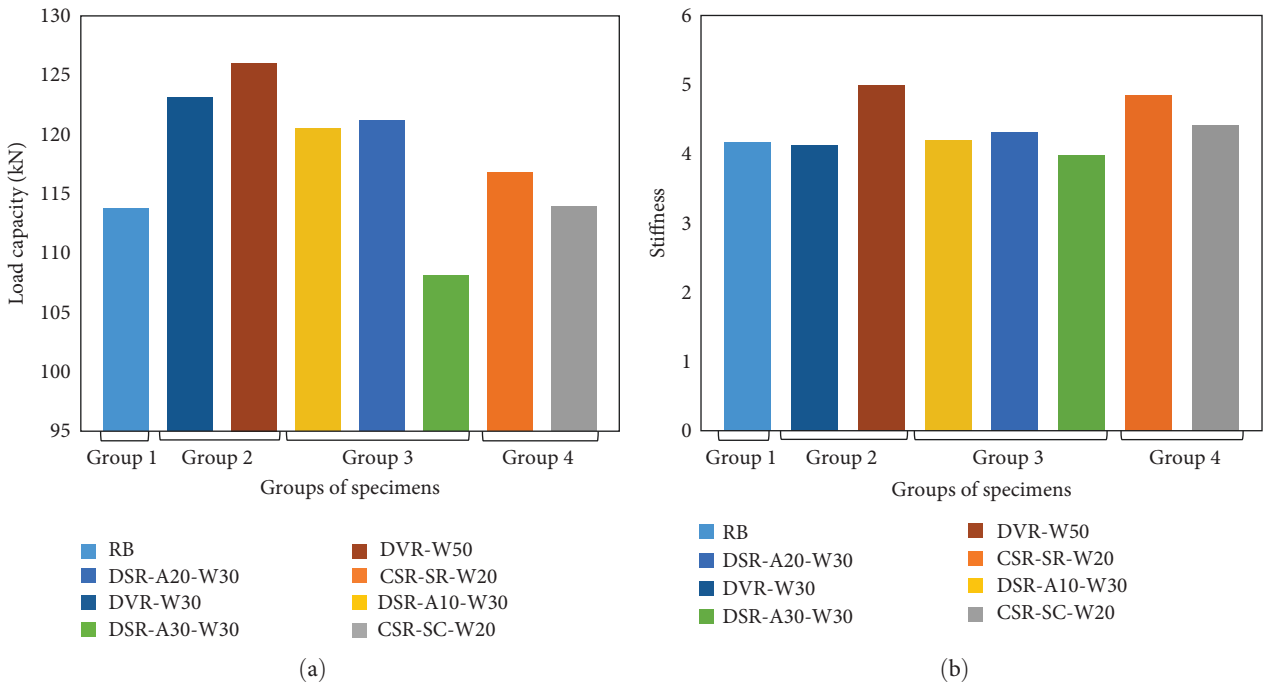

Figure 13: Comparison between specimen's behavior in bending: (a) load capacity; (b) stiffness.

beams with the confined concrete, in comparison with the RB. As the formation of any crack corresponds to spending an amount of energy, it is expected to have more energy dissipation in the confined specimens.

5.2. Load-Deflection Curves, Load Capacity, and Stiffness. To investigate the effects of the confinement configurations on the flexural performance of the beam, the load-deflection curves of all eight beam specimens are presented in Figure 11. The load-deflection curves of each group of specimens are separately illustrated in Figure 12.

As can be seen from Figure 11, most specimens have shown better flexural performance than that of the RB. Moreover, mostly had a fatter load-deflection curve. So, the best flexural performance was expected from DVR-W50, DSR-A10-W30, and CSR-SC-W20 through load-deflection curves. Meanwhile, some specimens showed a few improvements in load capacity, while some of them had less load capacity than the RB. The load-deflection curves of the second group specimens are illustrated in Figure 12(b). The first branch of both curves is close to each other, while the second branches show different results. Although the second branch

Table 8: Specimen energy dissipation parameters.

Group	Specimen	Elastic energy[a] (kN.mm)	Plastic energy[b] (kN.mm)	Total energy[c] (kN.mm)
Group 1	RB	1,606.4	910.4	2,516.8
Group 2	DVR-W30	1,893.5 (+%17.9)[d]	1,029.1 (+%13)	2,922.7 (+%16.12)
	DVR-W50	1,700.4 (+%5.8)	3,199.9 (+%251)	4,900.3 (+%94.7)
Group 3	DSR-A10-W30	1,838.2 (+%14.4)	3,078.9 (+%238)	4,917.1 (+%95.37)
	DSR-A20-W30	1,743 (+%8.5)	1,163.8 (+%27.8)	2,906.8 (+%15.5)
	DSR-A30-W30	1,529.7 (−%4.8)	1,144.1 (+%25.7)	2,673.8 (+%6.24)
Group 4	CSR-SR-W20	1,490.2 (−%7.2)	1,425.5 (+%56.6)	2,915.7 (+%15.85)
	CSR-SC-W20	1,529.1 (−%4.8)	2,138 (+%135)	3,667.2 (+%45.71)

[a]Area under the elastic zone of the load-deflection curve, [b]area under the plastic zone of the load-deflection curve up to 80% of the maximum load in the second branch, [c]sum of elastic and plastic energy, [d]percentages of changes compared to the reference beam.

of DVR-W30 is sharp descending, this branch in DVR-W50 exhibits a smooth tilt. In other words, the area under the first branch (ascending branch) of both specimens is nearly the same, while this area under the second branch of DVR-W50 is much higher than that of DVR-W30. In comparison between the flexural behavior of the third group shown in Figure 12(c), the first branch in all three specimens is ascending with slopes close to each other. In the case of the second branch, DSR-A30-W30 had a straight descending line, but in both DSR-A20-W30 and DSR-A10-W30, after sudden load decrease, the horizontal branch is shown yielding performance. DSR-A10-W30 had a much longer yield zone than DSR-A20-W30. Thus, satisfying ductility was expected from DSR-A10-W30. On the other hand, there is a negligible difference in load capacity of DSR-A10-W30 and DSR-A20-W30, while DSR-A30-W30 load capacity had about 10% reduction than DSR-A10-W30. Fourth group load-deflection curves are illustrated in Figure 12(d). According to the curves, CSR-SR-W20 tolerates more load than CSR-SC-W20. In both specimens, the second branch is sharply descending and continues with a hardening zone before failure. However, the second branch in CSR-SR-W20 was longer than CSR-SC-W20, so hardening behavior accrued sooner in CSR-SC-W20, while the hardening zone appeared after 80% of the failure load in CSR-SR-W20. Thus, the hardening area of CSR-SR-W20 occurred after the ultimate load and practically cannot be used in ductility calculations.

Maximum load capacity and stiffness of beams are other important parameters of flexural behavior. Based on the results, Table 7 and Figure 13 were prepared to compare the effects of confinement on load capacity and stiffness of specimens. According to Table 7 and Figure 13, negligible variation is observed except in DVR-W50, which shows 10.75% and 25.25% improvement in load-carrying capacity and stiffness compared to the RB, respectively. On the other hand, DVR-W30 tolerates more load with about 8% improvement. Thus, it could be concluded that confinement in the discrete vertical manner (second group) is more effective on load-carrying capacity.

5.3. Energy Dissipation. Energy dissipation is one of the important characteristics of flexural behavior which shows the energy absorbed by the beam before its failure. First, the bilinear curves were plotted, so elastic energy and plastic energy were calculated separately. Table 8 shows the results of energy dissipation calculations of specimens, and Figure 14 compares the energy dissipation between specimens. In these computations, the ultimate point was taken at 80% of the maximum load in the second branch.

According to Table 8 and Figure 14(a), there are negligible changes in elastic energy dissipation of confined specimens compared to the RB; however, about 18% improvement and a 7.2% decrease in DVR-W30 and CSR-SR-W20 were observed, respectively. Thus, compression zone confinement in the elastic branch of beam flexural behavior has negligible effects on energy dissipation. On the other hand, enormous improvement was seen in the plastic energy dissipation of some confined specimens compared with the RB. DVR-W30, DSR-A10-W30, and CSR-SC-W20 absorbed 251%, 238%, and 135% more plastic energy than RB, respectively. The reason for energy dissipation improvement was functional confinement that resisted compression by limiting side expansion. Thus, many tiny horizontal and vertical cracks showed up instead of a few wide cracks. These tiny cracks absorbed too much energy to have occurred. Meanwhile, all confined specimens absorbed more total energy and plastic energy than the RB, but the three confined specimens had enormous higher energy absorption, which shows the effectiveness of confinement.

Unconfined concrete has limited ductility, and after about 0.8 Pmax, the absorption of energy is negligible. However, in those with more ductile features, the energy absorption continues up to the failure point. Naaman and Jeong

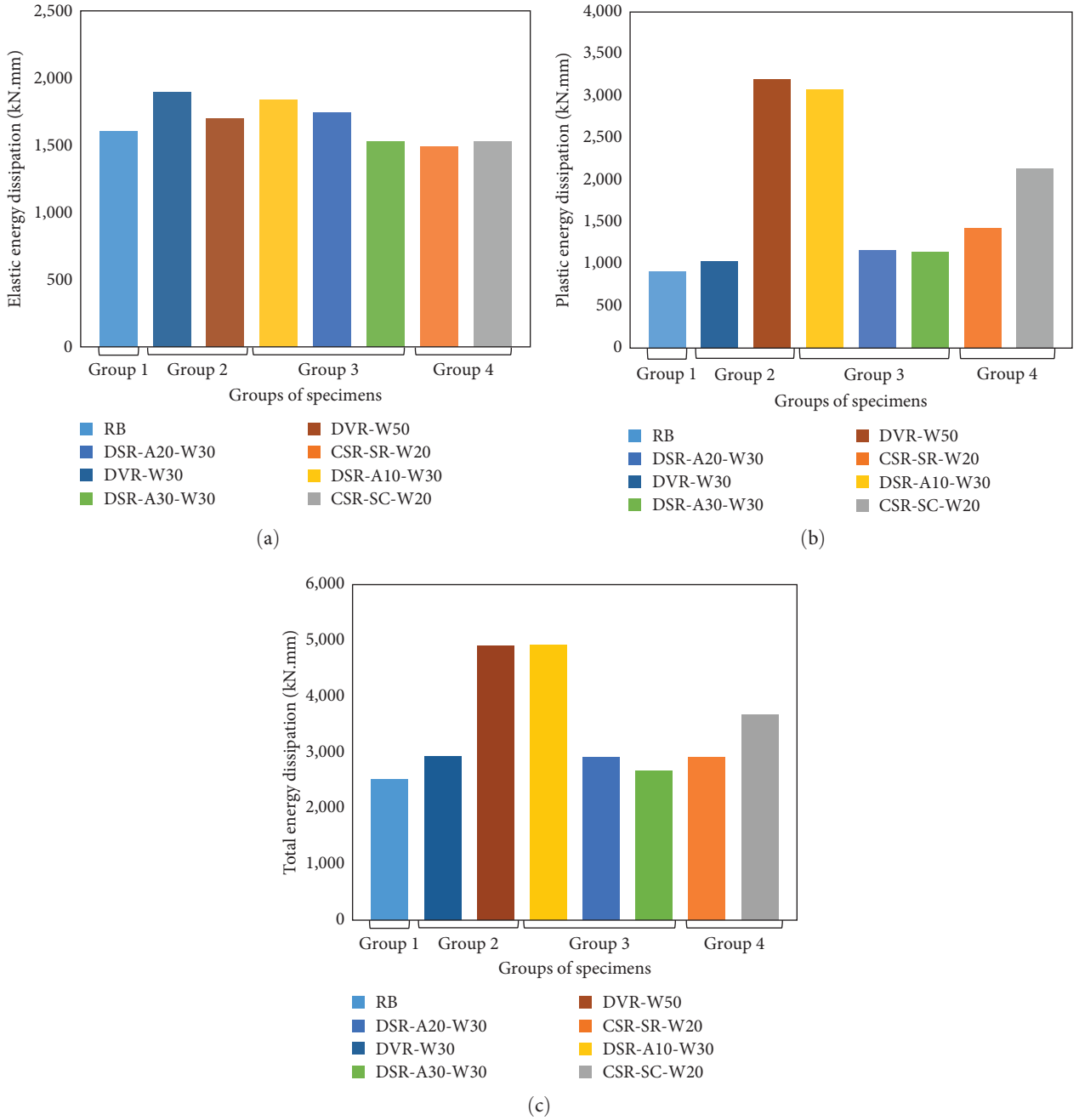

Figure 14: Compare energy dissipation up to 80% of the failure load between specimens: (a) elastic energy dissipation; (b) plastic energy dissipation; (c) total energy dissipation.

[51] defined the ultimate point at Pmax, 80% of the failure load in the second branch or up to the failure point in FRP-RC beams. Thus, energy dissipations are recalculated with the failure point as the ultimate point consideration. The results of energy dissipation of specimens with failure point consideration as the ultimate point are illustrated and compared in Table 9 and Figure 15.

According to Table 9 and Figure 15 and comparing them with Table 8 and Figure 14, elastic energy dissipation had no difference, while enormous improvement was achieved with Naaman's recommendation [51] in plastic and total energy dissipation. Results revealed that plastic energy could be improved up to 268% compared to the RB by DVR-W50, and the greatest improvement in total energy dissipation was observed in DSR-A10-W30 with a 109.8% increase compared to the RB. Meanwhile, the least improvement of plastic and total energy dissipation was seen in DVR-W30 with 20.4% and 18.8% compared to the RB, respectively. Generally, it could be concluded that the confinement of the compression zone had an effective influence on the ultimate point which appeared in energy dissipation results.

5.4. Ductility. In this section, according to the load-deflection response and its bilinear curve results, the ductility of the

Table 9: Specimens energy dissipation parameters up to the failure point.

Group	Specimen	Elastic energy[a] (kN.mm)	Plastic energy[b] (kN.mm)	Total energy[c] (kN.mm)
Group 1	RB	1,606.4	989.7	2,596.1
Group 2	DVR-W30	1,893.5 (+%17.9)[d]	1,191.4 (+%20.4)	3,084.9 (+%18.8)
	DVR-W50	1,700.4 (+%5.8)	3,642.9 (+%268)	5,343.3 (+%105.8)
Group 3	DSR-A10-W30	1,838.2 (+%14.4)	3,608.5 (+%265)	5,446.7 (+%109.8)
	DSR-A20-W30	1,743 (+%8.5)	2,433.9 (+%146)	4,177 (+%60.9)
	DSR-A30-W30	1,529.7 (−%4.8)	2,096.9 (+%39.7)	3,626.6 (+%39.7)
Group 4	CSR-SR-W20	1,490.2 (−%7.2)	2,378.4 (+%140)	3,868.6 (+%49)
	CSR-SC-W20	1,529.1 (-%4.8)	2,596.75 (+%159)	4,091.9 (+%57.6)

[a]Area under the elastic zone of load-deflection curve, [b]area under the plastic zone of load-deflection curve up to the failure point, [c]sum of elastic and plastic energy, [d]percentages of changes compared to the reference beam.

confined beams is calculated and compared with that of the RB in two recommended methods:

(1) Ductility index (μ_Δ) is the ability of structural elements to sustain inelastic deformation before collapse, which is defined as the ratio of ultimate deflection to yield deflection. This definition was formulated by Oudah and El-Hacha [52] as follows:

$$\mu_\Delta = \frac{\Delta_u}{\Delta_y}, \tag{1}$$

where μ is the ductility index, Δ_u is ultimate deflection at the ultimate load (defined as load corresponding to 80% of maximum load at the second branch) Δ_y is the elastic deflection which is considered deflection corresponding to 75% of the peak load at the first branch.

(1) Ductility index (μ_E) is the conventional ductility index for elastoplastic behavior measured by energy dissipation is recommended by Naaman and Jeong [51] as follows:

$$\mu_E = \frac{1}{2}\left(\frac{E_{\text{tot}}}{E_{el}} + 1\right), \tag{2}$$

where μ_E is ductility index, E_{tot} is the total energy that is the area under the load–deflection curve up to the ultimate load (ultimate load defined as either maximum load, load at failure, or load corresponding to 80% of maximum load at the second branch) and E_{el} is the elastic energy. In this study, the ultimate load is considered as failure load which is recommended to have a better presentation of confinement influence.

Structural ductility is the main concern in FRP-RC beams due to the elastic behavior of FRP materials up to the rupture without yielding branches. Thus, both definitions of ductility are calculated and represented in Table 10. Then, for better comparison between specimens, Figure 16 is prepared.

According to Table 10 and Figure 16, there is a negligible difference between the two ductility method results of the RB, while the ductility index based on energy dissipation had a better presentation of the confinement effect. To compare the specimen ductility, most of the confined specimens have a significant increment in ductility up to 60%. On average, the results of the three groups of confined beams show improvement in ductility compared to the RB. Based on the results, DVR-W50, DSR-A10-W30, and CSR-SC-W20, respectively, had about 60%, 50%, and 40% ductility improvement regardless of confinement method (continues/discrete or vertical/spiral), while other specimens, including CSR-SR-W20, DSR-A20-W30, and DSR-A30-W30 increased the ductility up to 37.5%, 29.8%, and 28.8% compared to RB, respectively. On the other hand, the non-ductile behavior of DVR-W30 with only 0.5% improvement, reveals that the effective parameter to improve ductility is the ribbon width and the free space between them. If ribbons were too close or too far from each other, confinement shall not be functional.

Based on the records, Figures 17 and 18 are prepared to compare the effects of width and the free space between confinement ribbons on ductility and energy dissipations. According to Figure 17, ribbon width may not be effective on ductility while the free space between them influenced the ductility and energy dissipation. Regarding Figures 18(a) and 18(b), if ribbons are too close to each other, act like a cold joint, and failure occurs before the confinement operates. On the other hand, by increasing the free space between ribbons more than the specific distance, a reduction was observed in

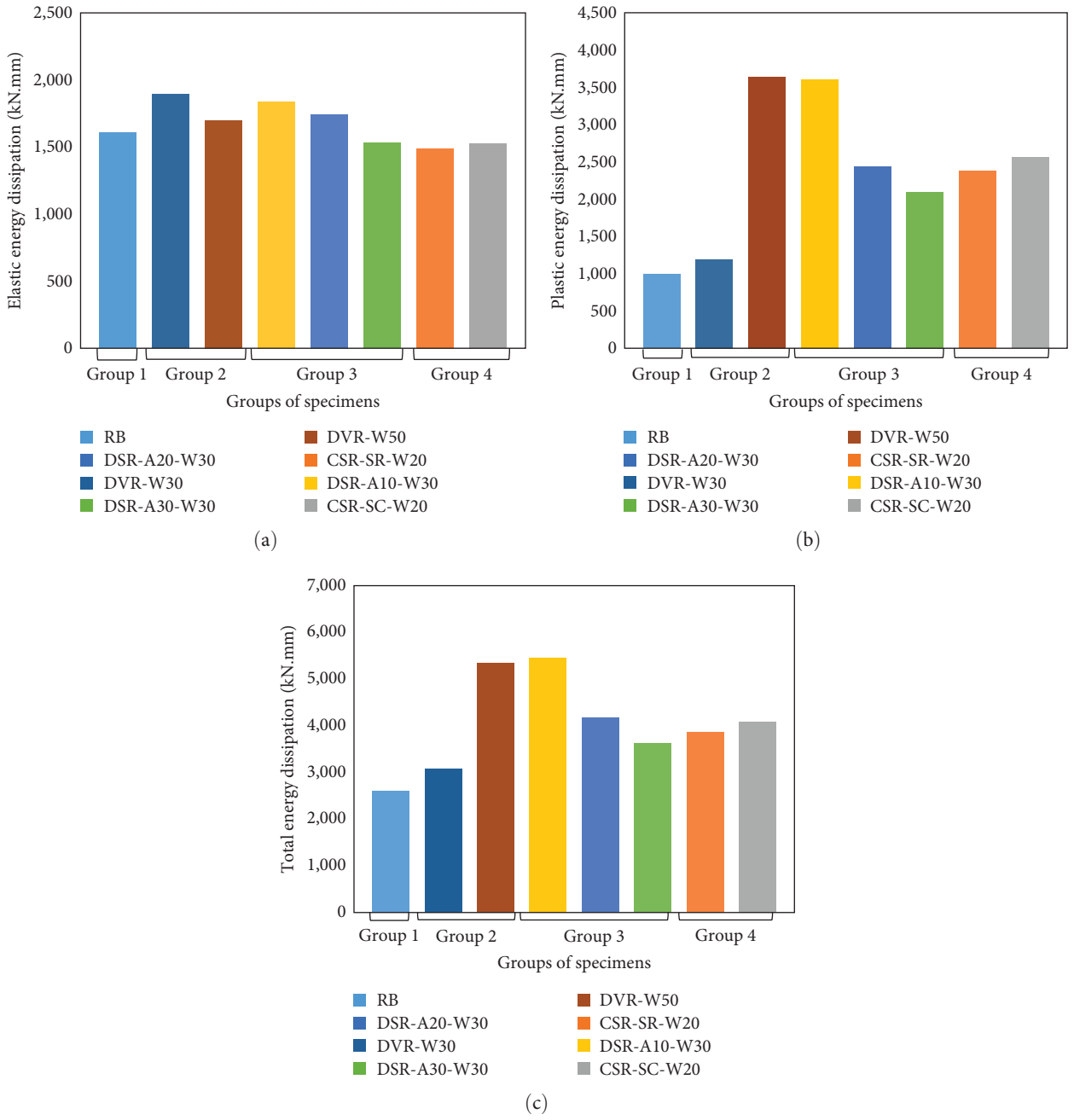

Figure 15: Comparing the energy dissipation up to the failure point between specimens: (a) elastic energy dissipation; (b) plastic energy dissipation; (c) total energy dissipation.

ductility, which was followed by steady ductility. Thus, It could be concluded that there is an optimum free space between ribbons that could provide the greatest ductility and energy dissipation in confinement FRP-RC beams.

To provide identical conditions between specimens, Figures 19(a) and 19(b) are presented to illustrate the effect of free space between ribbons on ductility and energy dissipation only in those specimens that had ribbons with 30 mm width, respectively. In this case with the specific beam dimension, confinement height of 75 mm, and ribbon width of 30 mm, it seems like the optimum free space between confining ribbons should be considered at about 50 mm.

5.5. Strain Gauge Results. During the specimen's construction and tests, strain gauges were mostly disconnected. Thus, unfortunately, the results of strain gauges are not useful for comparison and conclusion. Meanwhile, Figure 20 illustrates the strain–load curve of Five confined specimens of longitudinal GFRP reinforcement during the test. Based on Figure 20, the linear behavior of GFRP bars is concluded, while it is clear that failure in all specimens occurred at compression concrete before GFRP bars reached their ultimate point. Thus, confinement in the compression zone of concrete has no effect on longitudinal bar behavior. So, it is likely that no specific consideration is needed during the longitudinal bar design of

Table 10: Specimen ductility parameters.

Group	Specimen	μ_{Δ}[a]	μ_{E}[b]
Group 1	RB	1.30	1.31
Group 2	DVR-W30	1.30 (−%0.65)[c]	1.31 (+%0.5)
	DVR-W50	2.09 (+%59.99)	2.07 (+%58.3)
Group 3	DSR-A10-W30	1.96 (+%50.18)	1.98 (+%51.5)
	DSR-A20-W30	1.37 (+%4.86)	1.7 (+%29.8)
	DSR-A30-W30	1.42 (+%8.6)	1.68 (+%28.8)
Group 4	CSR-SR-W20	1.53 (+%17.63)	1.8 (+%37.5)
	CSR-SC-W20	1.82 (+%39.43)	1.84 (+%40.5)

[a]Ductility index expression by deflection, [b]ductility index expression by Energy dissipation, [c]percentages of changes compared to the reference beam.

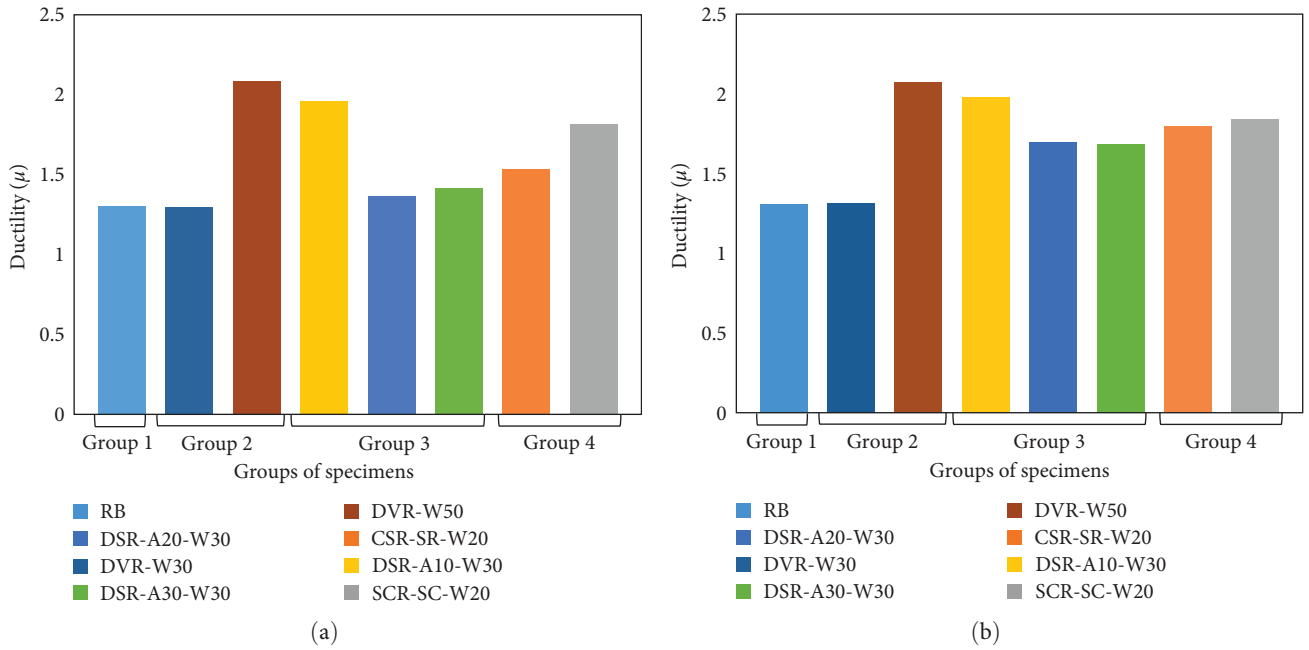

Figure 16: Comparing ductility between specimens: (a) μ_{Δ}; (b) μ_{E}.

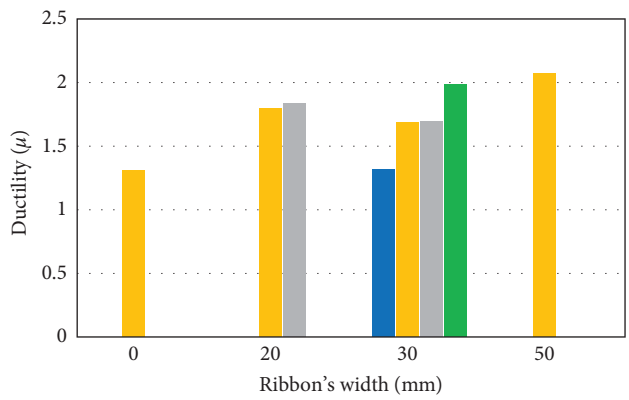

Figure 17: Effect of ribbon width on ductility.

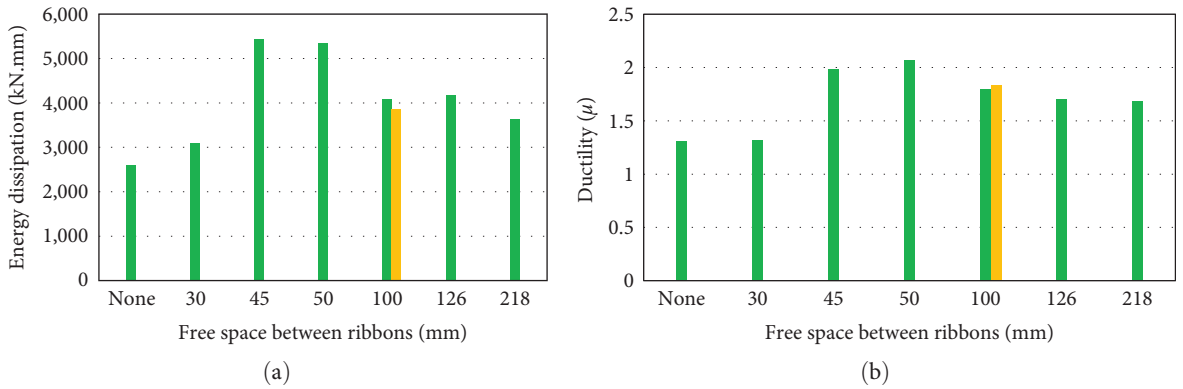

Figure 18: Effect of free space between ribbons on (a) energy dissipation and (b) ductility.

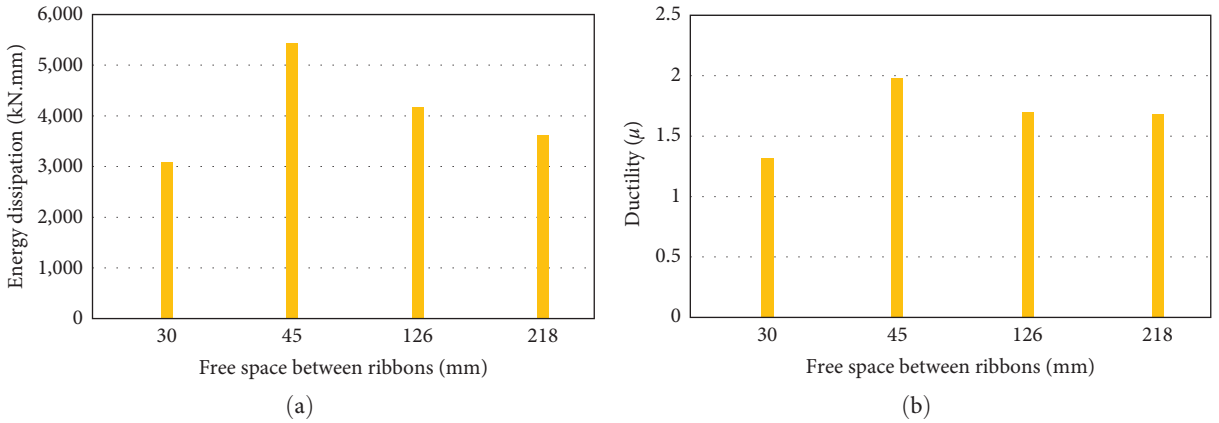

Figure 19: Effect of free space between ribbons with 30 mm of width on (a) energy dissipation and (b) ductility.

confinement beams except in those where the maximum load-carrying capacity improved.

6. Conclusions

In this study, the flexural behavior of GFRP over-RC beams confined by CFRP sheets has been investigated. Eight half-scale beam specimens, including one RB and seven confined beams with three different methods of confinement (in three groups) in different ribbon widths and different free spaces between confined ribbons, were tested. In confined specimens, CFRP sheets are confined only to the compression zone of the concrete beam. Different aspects of confinement effects on the flexural behavior of FRP-RC beam, including ductility load carrying capacity, etc., were discussed. From this study, the following results can be concluded:

(i) The test results have indicated that most of the confined specimens improved load-carrying capacity. The most load-carrying capacity showed up in DVR-W50 with about an 11% increase, and the least one appeared in DSR-A30-W30 with about a 5% decrease. On the other hand, it could be concluded that the confined method of the second group (discrete vertical manner) has the best effect on load-carrying capacity, which both specimens of this group had the greatest improvement.

(ii) The amount of energy dissipation of all confined specimens was higher than the RB, in which DSR-A10-W30 (specimen of Group 3) was about 110% higher than the RB total energy dissipation. On the other hand, the plastic energy of DVR-W50 was much higher than the RB, and up to about 268% improvement was observed, respectively.

(iii) Based on the values of the ductility parameters obtained from the load–deflection curve, ductility indices of DVR-W50, DSR-A10-W30, and CSR-SC-W20 showed significant improvement up to about 60%, 50%, and 40% in comparison of references beam, respectively. It could be concluded that the confinement method (discrete/continuous and vertical/diagonal) did not affect ductility. But, the ribbon width, space between ribbons, and the height of confinement are the effective parameters that should be noticed.

(iv) Based on the experimental observations and obtained results, confinement of concrete compression zone in FRP over-RC beams, could result in increasing ductility, and have benefits like easy application, low cost

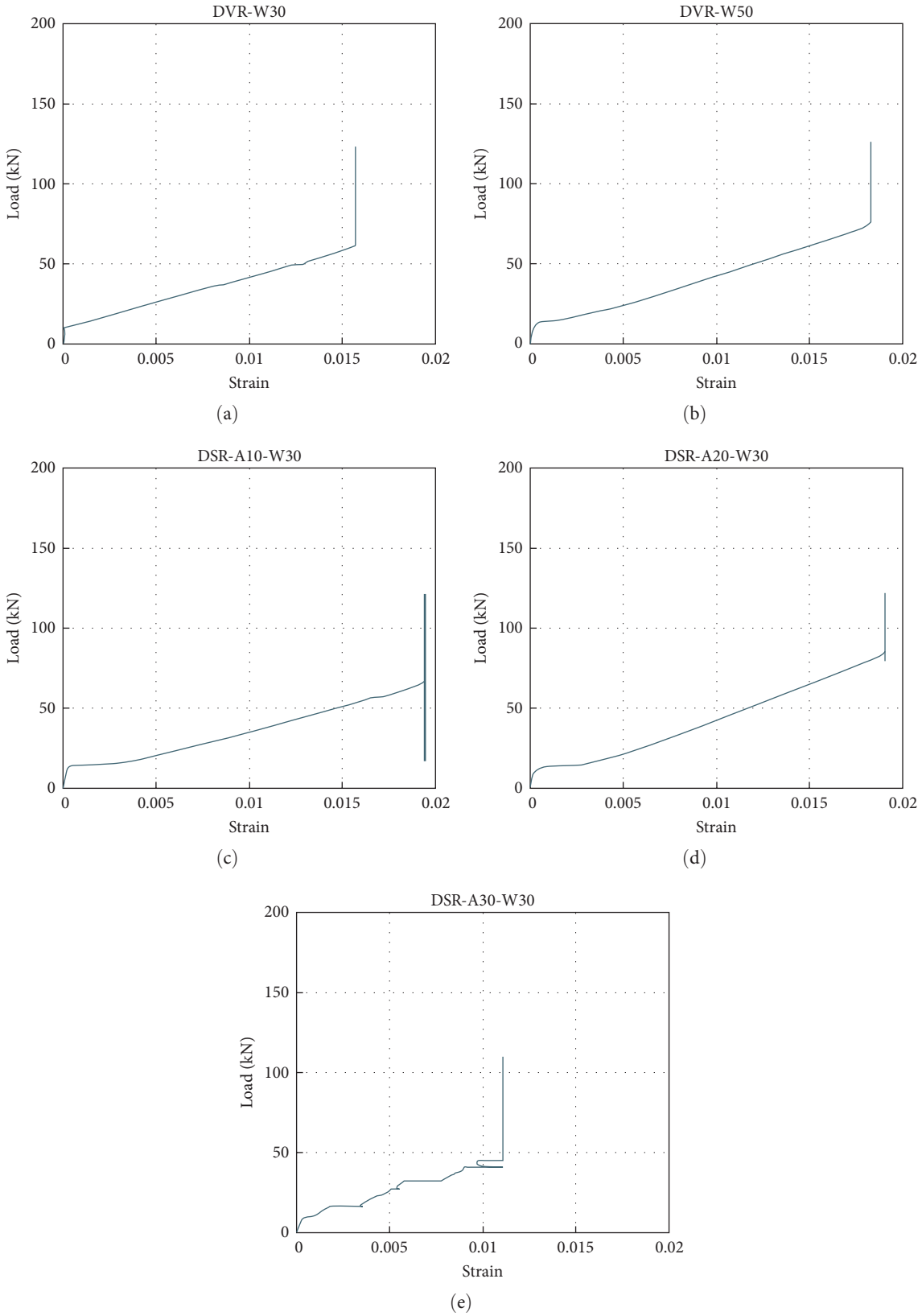

Figure 20: Load-strain curves of GFRP bars embedded in specimens: (a) DVR-W30; (b) DVR-W50; (c) DSR-A10-W30; (d) DSR-A20-W30; and (e) DSR-A30-W30.

compared to ECC, and corrosion resistance properties compared to the most practical fibers in FRC.

(v) The confinement method of Group 4 (beams confined with continuous spiral CFRP ribbon in 20 mm width) provides acceptable improvement on ductility and energy dissipation, while the precast confinement is practically easy to apply to the reinforcement before concrete casting.

Since novel ideas have been researched in this study, authors tend to find out if the idea is practical and improves the flexural behavior of FRP-RC beams. Thus, more research has been required to discover optimized width, height, and free space of confinement.

Data Availability

The data used to support the findings of this study are included in the article.

Conflicts of Interest

The authors declare that they have no known competing financial interests or personal relationships that could have appeared to influence the work reported in this paper.

Acknowledgments

The support provided by Shahrood University of Technology is gratefully acknowledged.

References

[1] Y. Zhou, J. Zhang, W. Li, B. Hu, and X. Huang, "Reliability-based design analysis of FRP shear strengthened reinforced concrete beams considering different FRP configurations," *Composite Structures*, vol. 237, Article ID 111957, 2020.

[2] H. Baji, H. R. Ronagh, and C.-Q. Li, "Probabilistic assessment of FRP-confined reinforced concrete columns," *Composite Structures*, vol. 153, pp. 851–865, 2016.

[3] B. Benmokrane, O. Chaallal, and R. Masmoudi, "Glass fibre reinforced plastic (GFRP) rebars for concrete structures," *Construction and Building Materials*, vol. 9, no. 6, pp. 353–364, 1995.

[4] I. F. Kara and A. F. Ashour, "Flexural performance of FRP reinforced concrete beams," *Composite Structures*, vol. 94, no. 5, pp. 1616–1625, 2012.

[5] I. F. Kara and A. F. Ashour, "Moment redistribution in continuous FRP reinforced concrete beams," *Construction and Building Materials*, vol. 49, pp. 939–948, 2013.

[6] A. E. El-Sisi, A. Saucier, H. A. Salim, and J. M. Hoemann, "Experimental and numerical evaluation of reinforced concrete walls retrofit systems for blast mitigation," *Journal of Performance of Constructed Facilities*, vol. 33, no. 2, Article ID 4018113, 2019.

[7] A. H. Elbelbisi, A. A. El-Sisi, H. A. Hassan, H. A. Salim, and H. F. Shabaan, "Parametric study on steel–concrete composite beams strengthened with post-tensioned cfrp tendons," *Sustainability*, vol. 14, no. 23, Article ID 15792, 2022.

[8] A. A. El-Sisi, H. M. El-Emam, A. E.-M. I. El-Kholy, S. S. Ahmad, H. M. Sallam, and H. A. Salim, "Structural behavior of RC beams containing unreinforced drilled openings with and without CFRP strengthening," *Polymers*, vol. 14, no. 10, 2022.

[9] F. M. Mukhtar and M. E. Shehadah, "Shear behavior of flexural CFRP-strengthened RC beams with crack-induced delamination: experimental investigation and strength model," *Composite Structures*, vol. 268, Article ID 113894, 2021.

[10] F. M. Mukhtar, A. Jawdhari, and A. Peiris, "Mixed-mode FRP—concrete bond failure analysis using a novel test apparatus and 3D nonlinear FEM," *Journal of Composites for Construction*, vol. 26, no. 6, Article ID 4022082, 2022.

[11] R. Graça-e-Costa, F. M. Mukhtar, and D. Dias-da-Costa, "Mesh-independent framework for the bidimensional analysis of CFRP—concrete debonding shear tests with discrete fracture," *Journal of Composites for Construction*, vol. 26, no. 3, Article ID 4022030, 2022.

[12] M. N. Habeeb and A. F. Ashour, "Flexural behavior of continuous GFRP reinforced concrete beams," *Journal of Composites for Construction*, vol. 12, no. 2, pp. 115–124, 2008.

[13] A. F. Ashour and M. N. Habeeb, "Continuous concrete beams reinforced with CFRP bars," *Proceedings of the Institution of Civil Engineers*, vol. 161, no. 6, pp. 349–357, 2008.

[14] C. Barris, L. Torres, A. Turon, M. Baena, and A. Catalan, "An experimental study of the flexural behaviour of GFRP RC beams and comparison with prediction models," *Composite Structures*, vol. 91, no. 3, pp. 286–295, 2009.

[15] A. Nanni, "North American design guidelines for concrete reinforcement and strengthening using FRP: principles, applications and unresolved issues," *Construction and Building Materials*, vol. 17, no. 6-7, pp. 439–446, 2003.

[16] ACI Committee 440, *ACI 440-1R-15 Guide for the design and construction of concrete reinforced with Fiber Rienforced Polymers FRP (bars)*, 2015.

[17] M. A. Adam, M. Said, A. A. Mahmoud, and A. S. Shanour, "Analytical and experimental flexural behavior of concrete beams reinforced with glass fiber reinforced polymers bars," *Construction and Building Materials*, vol. 84, pp. 354–366, 2015.

[18] H. G. Harris, W. Somboonsong, and F. K. Ko, "New ductile hybrid FRP reinforcing bar for concrete structures," *Journal of Composites for Construction*, vol. 2, no. 1, pp. 28–37, 1998.

[19] W. Qu, X. Zhang, and H. Huang, "Flexural behavior of concrete beams reinforced with hybrid (GFRP and steel) bars," *Journal of Composites for Construction*, vol. 13, no. 5, pp. 350–359, 2009.

[20] M. A. Aiello and L. Ombres, "Structural performances of concrete beams with hybrid (fiber-reinforced polymer-steel) reinforcements," *Journal of Composites for Construction*, vol. 6, no. 2, pp. 133–140, 2002.

[21] D. Lau and H. J. Pam, "Experimental study of hybrid FRP reinforced concrete beams," *Engineering Structures*, vol. 32, no. 12, pp. 3857–3865, 2010.

[22] Z. Li, H. Zhu, X. Zhen, C. Wen, and G. Chen, "Effects of steel fiber on the flexural behavior and ductility of concrete beams reinforced with BFRP rebars under repeated loading," *Composite Structures*, vol. 270, Article ID 114072, 2021.

[23] H. Wang and A. Belarbi, "Ductility characteristics of fiber-reinforced-concrete beams reinforced with FRP rebars," *Construction and Building Materials*, vol. 25, no. 5, pp. 2391–2401, 2011.

[24] E. Aydın, E. Boru, and F. Aydın, "Effects of FRP bar type and fiber reinforced concrete on the flexural behavior of hybrid beams," *Construction and Building Materials*, vol. 279, Article ID 122407, 2021.

[25] J. Cai, J. Pan, and X. Zhou, "Flexural behavior of basalt FRP reinforced ECC and concrete beams," *Construction and Building Materials*, vol. 142, pp. 423–430, 2017.

[26] E. N. Herbert and V. C. Li, "Self-healing of microcracks in engineered cementitious composites (ECC) under a natural environment," *Materials*, vol. 6, no. 7, pp. 2831–2845, 2013.
[27] V. C. Li and S. Wang, "Flexural behaviors of glass fiber-reinforced polymer (GFRP) reinforced engineered cementitious composite beams," *Journal of Materials Science*, vol. 99, no. 1, pp. 11–21, 2002.
[28] W. Ge, "Experimental study on flexural behavior of ECC-concrete composite beams reinforced with FRP bars," *Composite Structures*, vol. 208, pp. 454–465, 2019.
[29] F. Yuan and J. L. Pan, "Experimental study on flexural behaviors of engineered cementitious composite beams reinforced with FRP bars," in *8th International Conference on Fracture Mechanics of Concrete and Concrete Structures FraMCoS*, pp. 10–14, Collage of Civil and Transportation Engineering, Shenzhen University, Spain, March 2013.
[30] Y.-F. Wu, "New avenue of achieving ductility for reinforced concrete members," *Journal of Structural Engineering*, vol. 132, no. 9, pp. 1502–1506, 2006.
[31] Y. W. Zhou, Y. F. Wu, J. G. Teng, and A. Y. T. Leung, "Parametric space for the optimal design of compression-yielding FRP-reinforced concrete beams," *Materials and Structures*, vol. 43, no. 1-2, pp. 81–97, 2010.
[32] Y.-F. Wu, Y.-W. Zhou, and X.-Q. He, "Performance-based optimal design of compression-yielding FRP-reinforced concrete beams," *Composite Structures*, vol. 93, no. 1, pp. 113–123, 2010.
[33] Y. W. Zhou, Y. F. Wu, J. G. Teng, and A. Y. T. Leung, "Ductility analysis of compression-yielding FRP-reinforced composite beams," *Cement and Concrete Composites*, vol. 31, no. 9, pp. 682–691, 2009.
[34] X. C. Liu, Y. F. Wu, A. Y. T. Leung, and J. G. Hou, "Mechanical behavior of mild steel compressive yielding blocks," in *Proceedings of the First Asia-pacific Conference on FRP in Structures*, pp. 12–14, Deptartment of Civil Engineering, University of Hong Kong, Hong Kong, China, 2007.
[35] J. C. M. Ho, J. Y. K. Lam, and A. K. H. Kwan, "Effectiveness of adding confinement for ductility improvement of high-strength concrete columns," *Engineering Structures*, vol. 32, no. 3, pp. 714–725, 2010.
[36] H. F. Isleem, Z. Wang, D. Wang, and S. T. Smith, "Monotonic and cyclic axial compressive behavior of CFRP-confined rectangular RC columns," *Journal of Composites for Construction*, vol. 22, no. 4, Article ID 4018023, 2018.
[37] J. G. Teng, Q. G. Xiao, T. Yu, and L. Lam, "Three-dimensional finite element analysis of reinforced concrete columns with FRP and/or steel confinement," *Engineering Structures*, vol. 97, pp. 15–28, 2015.
[38] N. A. Siddiqui, "Experimental investigation of RC beams strengthened with externally bonded FRP composites," *Latin American Journal of Solids and Structures*, vol. 6, no. 4, pp. 343–362, 2009.
[39] M. Nematzadeh, M. Mousavimehr, J. Shayanfar, and M. Omidalizadeh, "Eccentric compressive behavior of steel fiber-reinforced RC columns strengthened with CFRP wraps: experimental investigation and analytical modeling," *Engineering Structures*, vol. 226, Article ID 111389, 2021.
[40] A. Al-Khafaji, H. Salim, and A. El-Sisi, "Behavior of RC beams strengthened with CFRP sheets under sustained loads," *Structures*, vol. 33, pp. 4690–4700, 2021.
[41] G. Campione, "Influence of FRP wrapping techniques on the compressive behavior of concrete prisms," *Cement and Concrete Composites*, vol. 28, no. 5, pp. 497–505, 2006.
[42] Z. Wu, W. Li, and N. Sakuma, "Innovative externally bonded FRP/concrete hybrid flexural members," *Composite Structures*, vol. 72, no. 3, pp. 289–300, 2006.
[43] F. Mukhtar and A. Deifalla, "Shear strength of FRP reinforced deep concrete beams without stirrups: Test database and a critical shear crack-based model," *Composite Structures*, vol. 307, Article ID 116636, 2023.
[44] D. E. Dixon, J. R. Prestrera, G. R. U. Burg et al., "Standard practice for selecting proportions for normal heavyweight, and mass concrete (ACI 211.1-91) reapproved 1997," Reported by ACI Committee 211, pp. 1–38, 1991.
[45] ASTM Standard C33, "Standard specification for concrete aggregatesi," 1900.
[46] STANDARD, British, *Testing Hardened Concrete—Compressive Strength of Test Specimens*, pp. 12390–12393, BS EN, 2009.
[47] ASTM, "ASTM D7205/7205M-standard test method for tensile properties of fiber reinforced polymer matrix composite bars 1," vol. 62011.
[48] I. Standard, *International Standard 10406*, 2008.
[49] Quantom®, "Quantom structural systems and materials provider," https://quantom.ir/.
[50] ACI Committee 440, "440.2R-17: guide for the design and construction of externally bonded FRP systems for strengthening concrete structures," 2017.
[51] A. E. Naaman and M. Jeong, "45 structural ductility of concrete beams prestressed," in *Non-Metallic (FRP) Reinforcement for Concrete Structures: Proceedings of the Second International RILEM Symposium*, p. 379, CRC Press, 1995.
[52] F. Oudah and R. El-Hacha, "A new ductility model of reinforced concrete beams strengthened using fiber reinforced polymer reinforcement," *Composites Part B: Engineering*, vol. 43, no. 8, pp. 3338–3347, 2012.